

LABORATORY MEASUREMENTS OF WAVE ATTENUATION THROUGH MODEL AND LIVE VEGETATION

Y. Ozeren¹ and D. G. Wren²

ABSTRACT

Surge and waves generated by hurricanes and tropical storms often cause severe damage and loss of life in coastal areas. It is widely recognized that wetlands along coastal fringes reduce storm surge and waves. Yet, the potential role and primary mechanisms of wave mitigation by wetland vegetation are not fully understood. Knowledge of wave attenuation is essential for assessing the ability of vegetation to limit wave damage. The goal of the work reported here was to use a laboratory wave flume to quantify the attenuation of waves as a function of vegetation type, density, and height. The properties of waves passing through rigid and flexible model vegetation as well as live *Spartina alterniflora* and *Juncus roemerianus* were measured. An automated system was developed and used to generate regular and random waves and to record time series of water surface elevation. A technique was developed for extracting the water surface profile through the vegetation field from images recorded with a consumer grade digital video camera. The new method was also tested for wave setup measurements along a plane sloping beach.

Keywords: Vegetation, wave attenuation, energy dissipation, wetlands, marsh, image processing

INTRODUCTION

Wetlands provide habitat for a wide range of plant and animal species, and improve water quality (Lightbody and Nepf, 2006). Smooth cord grass (*Spartina alterniflora*) and black needlerush (*Juncus roemerianus*) are common grass species in tidal salt marshes of the Atlantic and Gulf coasts. Marsh areas reduce the energy of the coastal storm surges and waves and therefore increase sedimentation and deposition. Coastal regions are becoming more vulnerable to natural disasters due to urbanization and wetland loss. Since wetlands provide significant economic and ecological benefits, awareness of the value of wetlands for coastal protection has increased in recent years, creating a need for more knowledge of the appropriate scaling and arrangement to maximize surge and wave reduction benefits.

Numerous experiments examining the interaction of vegetation and flowing water have been undertaken, and a detailed summary can be found in Wu (2007). However, only a few experiments have been conducted with the goal of measuring the effect of vegetation on waves and for examining the interactions among waves and vegetation. Asano et al. (1988) conducted experiments on wave attenuation due to vegetation in a flume using flexible polypropylene strips as model vegetation. Gambi et al. (1990) studied flow speed reduction

¹ Corresponding author: Department of Biology, The University of Mississippi, University, MS 38677, yozeren@olemiss.edu

² USDA-ARS National Sedimentation Laboratory, 598 McElroy Drive, Oxford, MS 38655-1157, Daniel.Wren@ars.usda.gov

by *Zostera marina* L. (eelgrass) in a seawater flume, with the seagrass bed occupying 20 percent of the width of the flume. Nepf (1999) conducted laboratory and field experiments and presented a model for drag, turbulence, and diffusion within emergent vegetation covering a range of vegetation densities and Reynolds numbers. Augustin et al. (2009) conducted 2D and 3D laboratory experiments to measure wave attenuations through model vegetation. A relatively recent theoretical study by Dean and Bender (2006) has shown that vegetation may significantly reduce wave setup; however, this finding has not yet been validated by experiments.

The objective of the current study was to measure the attenuation of waves as a function of vegetation type, density, and height in a laboratory wave tank. Laboratory-based water surface displacement measurements usually make use of wave gauges at fixed stations which do not allow the spatial variability of the wave height to be resolved. A large array of gauges is necessary to correctly resolve the surf zone flow phenomenon. Wave gauges also can cause perturbations of the wave field. Video analysis can provide the spatial and temporal variation of the water surface profile with a reasonable resolution. Some earlier studies of wave profile video analysis include those of Bonmarin et al. (1989) and Ericson and Hanson (2005). The ongoing improvements in digital imaging technology offer an alternative method for laboratory data collection with an acceptable level of precision. In this study, a video camera was used to record the water surface profile along with traditional wave probes, and a video analysis procedure was developed to estimate the continuous variation of wave height through the vegetation field. The same procedure was also used to estimate the wave setup along a plane sloping beach.

MATERIALS AND METHODS

Experiments were conducted in a 20.6 m long, 0.69 m wide, and 1.22 m deep wave tank designed and constructed at the USDA-ARS National Sedimentation Laboratory in Oxford, Mississippi (Figure 1). Two types of paddles, one a variable-draft flap-type and the other a piston type, were used interchangeably to generate waves at four different water depths. The wave generator was controlled by a stepper motor that was operated by a custom computer program. A porous, parabolic wave absorber was constructed at the downwave end of the tank to minimize wave reflection. The test section was placed 11.5 m away from the wave generator and was 3.6 m long. The bottom of the wave tank was elevated by a 0.29 m plywood false floor so that plants could be placed in the test section. A ramp with a slope of 1/7 was built in front of the wave generator to provide a gradual transition.

Five one meter capacitance-type wave probes were used to measure water surface displacement. One of the probes was placed 3 m away from the paddle to measure the incident wave height, and the remaining four were distributed along the test section at 1.5 m intervals starting 0.5 m ahead of the vegetation field. The sampling rate of the wave probes was 30 Hz, and the resolution was 0.24 mm. A digital video camera was used to capture the water surface displacement along the test section through the clear polycarbonate sidewall. The camera had 29.97 Hz frame rate and 1920 x 1080 pixel resolution. It was positioned 6 m away from the wave tank wall and leveled with the free surface elevation. The field-of-view was 5.82 m along the wave tank, yielding approximately 3 mm/pixel resolution. Blue dye was added to the water to increase contrast with the white wall of the tank. Colored markers were placed on the Plexiglas wall to locate the wave probes and scale the data during the video analysis.

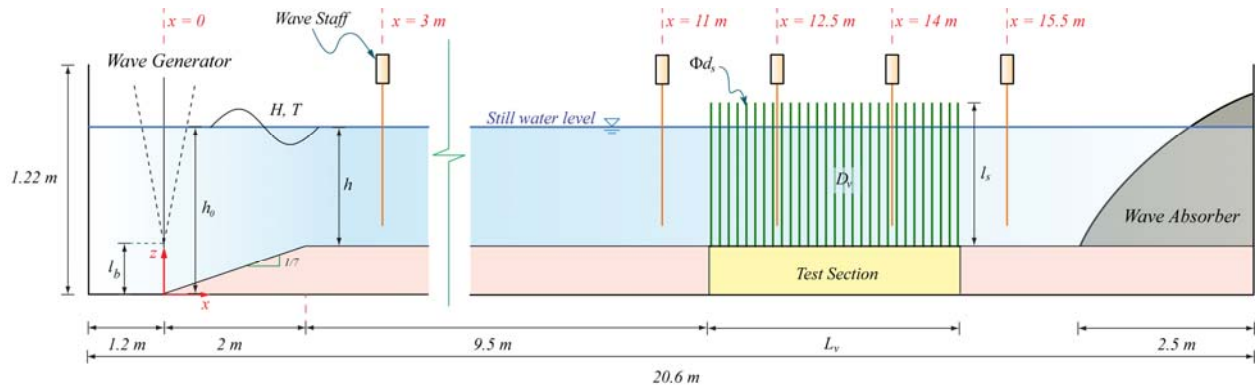


Figure 1. Definition sketch of the experimental setup.

Rigid and flexible model vegetation and live *S. alterniflora* and *J. Romerianus* were tested over a range of wave conditions and stem densities (Table 1 and 2). Rigid vegetation models were constructed from 9.5 mm diameter birch dowels by sliding them in a staggered pattern through the holes of two perforated 6.4 mm thick PVC sheets (Figure 2). The top sheet was leveled with the false floor and the remaining holes were sealed. Shortly after being immersed, the dowels swelled and locked in place without using any adhesive. EPDM foam rubber with a 9.5 mm diameter was used to construct flexible model vegetation. The EPDM foam rubber had a density of 368 kg/m^3 and a modulus of elasticity of 4 MPa. Strips of foam rubber 630 mm long were glued into the holes of the PVC sheets in a manner similar to that used for the rigid model vegetation, and the rest of the holes were again sealed.

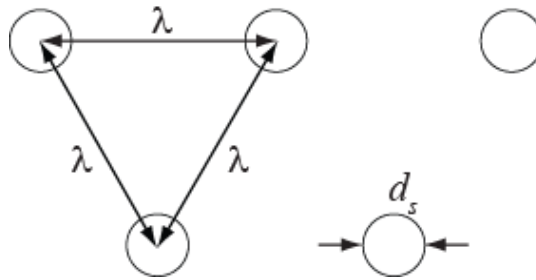


Figure 2. Model vegetation stem configuration. λ is the center-to-center distance between individual stems and d_s is the stem diameter.

Live *S. alterniflora* and *J. Romerianus* plants were collected from an outdoor nursery near Houma, LA, and transferred on site into six custom-built PVC boxes. The boxes were 686 mm wide, 610 mm long, 210 mm deep, and 286 mm high. Each box was divided into sixteen 170 mm by 152 mm cells. Plugs of vegetation with an approximately equal number of stems were placed into each cell to provide an even distribution and to control the stem density. The remaining gap around the plugs was filled with native soil. After being transferred into the wave tank, the plants were left under three 750 W growing lights 10 hours a day for 30 days. The wave tank was filled with fresh water up to just above the soil level during this recovery period. The temperature varied between 20°C - 24°C during the experiments.

Table 1. Ranges of wave parameters.

	Regular	Irregular
Wave height - H_i (H_{mo}) (m)	0.02 – 0.15	0.02 – 0.10
Wave period - T (T_p) (s)	0.7 – 2.0	0.7 – 1.8
Water depth - h (m)	0.4, 0.5, 0.6 and 0.7	0.5, 0.6 and 0.7

Table 2. Ranges of model parameters. Mean and standard deviations (in parenthesis) are given for live vegetation stem length and diameter values.

	Density – D_v (m^{-2}) / Spacing – λ (mm)	Stem length l_s (m)	Stem diameter d_s (mm)	Fractional coverage $a = D_v A_c$
Rigid model	156 / 86.1	0.63	9.4	0.011
	350 / 57.4	0.63		0.024
	350 / 57.4	0.48		0.024
	623 / 43.1	0.63		0.043
Flexible model	350 / 57.4	0.48	9.4	0.024
<i>S. alterniflora</i> (Green)	405	0.59 (0.21)	6.5 (0.9)	0.013
<i>J. romerianus</i> (Green)	2857	1.03 (0.27)	2.4 (0.6)	0.013

A plane wooden beach with a 1:20 slope was constructed over the existing false floor to investigate wave setup. The toe of the beach was at $x = 7.2$ m. The piston type wavemaker was used to generate regular waves. The previously described wave probes were mounted at 3 m, 7.5 m, 11 m, 12.5 m and 14 m away from the wave paddle to measure the water surface displacement.

Regular wave experiments were run for at least 100 wave cycles and repeated three times. Control runs with no vegetation in the flume were also performed. The time series of water surface displacements were filtered with a band-pass filter and analyzed using the zero down-crossing method to derive average wave height for regular waves. Irregular waves were generated using the JONSWAP spectrum. Five $100T_p$ long time series signals were generated for each spectrum for each vegetation configuration and for control runs to avoid uncertainties. Significant wave heights for irregular waves were calculated using spectral analysis by assuming the spectrum to be narrow banded and that the wave heights satisfied the Rayleigh distribution (Longuet-Higgins, 1952). Calculated wave heights were averaged over the steady portion of the recorded signal.

A subset of the experiments was recorded with a video camera. Each video recording began just before the wave generation and continued for 50 s for vegetation experiments and 100 s for wave setup experiments. The recorded videos were analyzed in three main steps: (1) video preprocessing, wherein the first few frames were analyzed to identify the still water level, wave gauge locations and the scaling parameters; (2) video processing, wherein the remaining frames were analyzed to identify the water surface; and (3) video postprocessing, wherein the water

surface data were analyzed. Each step is described in more detail below.

Video preprocessing: The first ten frames of the video were averaged and the red channel of the averaged frame was separated. This frame was cropped around the water surface and scale markers, which were on the flume sidewall as described previously. The red channel was converted into a black and white (binary) image with a user defined threshold and enhanced by removing unwanted imperfections through morphological operations. Background illumination was estimated by a series of smoothing operations. The probe locations were identified and scaling values were calculated using colored markers on the wave tank wall. It was observed that lens distortion error in the vertical direction was negligible for the area covered during the video recording. Therefore, only horizontal lens distortion was corrected using the known locations of the wave probe markers. Camera alignment was corrected using the initial free surface line (still water level) as the datum. Third order polynomials were fitted to the free surface line and the wave probe markers, to be used for camera distortion and alignment correction.

Video processing: The remaining frames were cropped around the still water level, and the red channel was separated. The estimated background from the preprocessing step was subtracted from each frame to obtain a uniform background. Each frame was then converted to a binary image with the previously defined threshold. The free surface was identified after enhancing the binary image through a series of morphological operations (Figure 3). The binary images were accumulated and averaged after the waves became steady. Free surface elevation data were scaled, normalized with the still water curve, and transformed along the horizontal axis to correct for curvature induced by the camera optics. Water surface displacements at the wave probe locations were interpolated from the estimated water surface profiles for each frame. Figure 4 shows a comparison of video and wave gauge data.

Video postprocessing: Each pixel value of the average frame, \mathbf{I} , represents the fraction of time that the pixel was dry. White regions in Figure 5 were always dry and black regions were always wet during the averaging period. The summation of the pixel values along a vertical line yields the variation of the mean water level along the horizontal axis. The vertical sums were normalized with respect to the still water level and scaled to calculate the mean water level. The average binary frame was transformed using the relation: $\mathbf{J} = \mathbf{I} \cdot (1 - \mathbf{I})$ to filter out the stationary pixels and capture the wave height envelope. The resulting matrix, \mathbf{J} , had values between 0 and 1 if the pixel value changed from frame to frame while it had zero values where there was no change. The average frame was then converted to a binary image with a threshold equal to:

$$e = \frac{1 - fT}{(fT)^2} \quad (1)$$

where f is the frame rate, which ensures that any change less frequent than the wave frequency is ignored. An example average frame is given in Figure 6. The region of non-zero values shows the wave height envelope. The thickness of the band defined by the threshold is the average wave height.

(a)

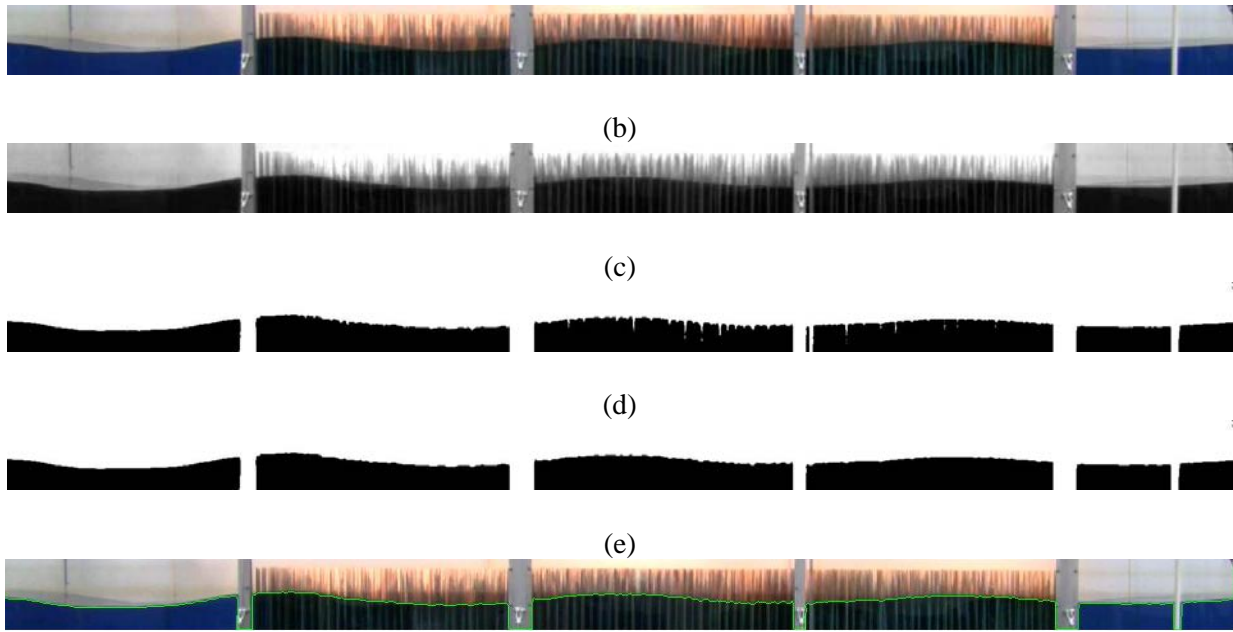


Figure 3. Summary of the video analysis procedure. (a) RGB image, (b) red channel, (c) binary image, (d) enhanced binary image and (e) the captured interface (green line).

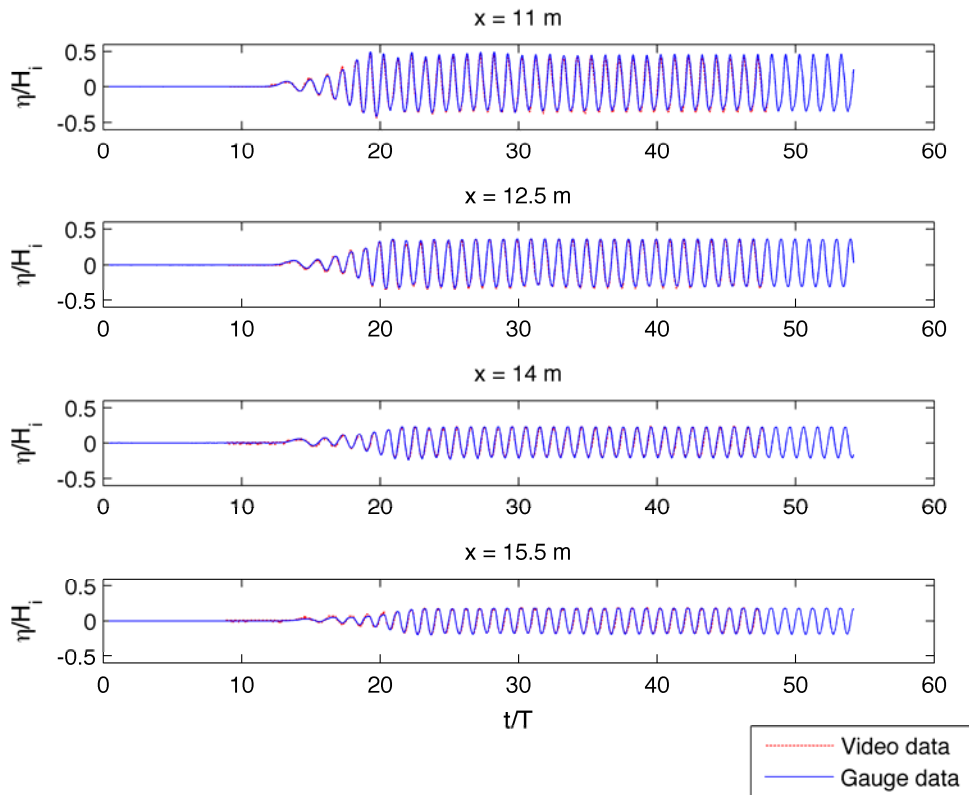


Figure 4. The wave probe time series data compared with the video data for rigid model vegetation ($T = 1.2$ s, $H_i = 0.1$ m, $h = 0.5$ m, $D_v = 623$ stems/ m^2 and $l_s = 0.63$ m).



Figure 5. A portion of the average (a) five frames and (b) 48 frames for breaking waves over the sloping beach ($T = 1.6$ s, $H = 0.14$ m and $h = 0.4$ m).

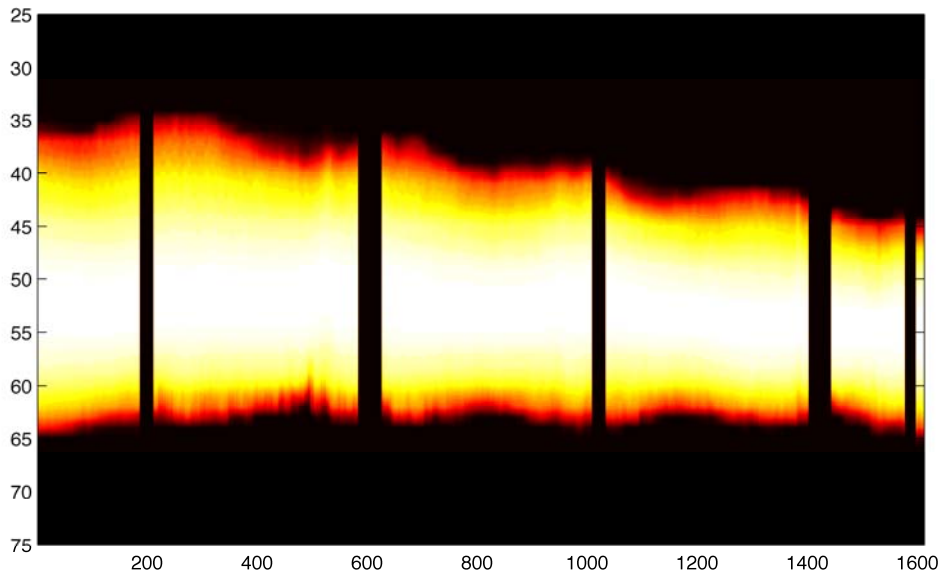


Figure 6. A sample transformed average frame for rigid model vegetation ($T = 1.2$ s, $H = 0.1$ m, $h = 0.5$ m and $D_v = 350$ stems/m² and $l_s = 0.63$ m). Vertical stripes are the supports of the wave tank, which blocked the camera's view of the water surface.

DISCUSSION OF RESULTS

Wave transmission data for rigid model vegetation are shown in Figure 7 for $H/L=0.03$, where H is wave height, L is wave length, and H/L is wave steepness. The wave height measured at the first gauge ($x = 11$ m) was assumed to be the incident wave height, H_i . Wave length was calculated from linear wave theory. In Figure 7a, three different densities (D_v) of vegetation are compared. The data sets with different wave lengths generally collapse well into single curves for value of D_v . It can be seen that most of the energy dissipation occurs within the first two wavelengths within the vegetation fields. In Figure 7b, the wave height evolution through model vegetation for regular and irregular waves is compared. Here, H refers to the significant wave height and the wave length is based on the peak wave period for irregular waves. Figure 7b shows that there was no significant difference in wave attenuation between regular and irregular waves.

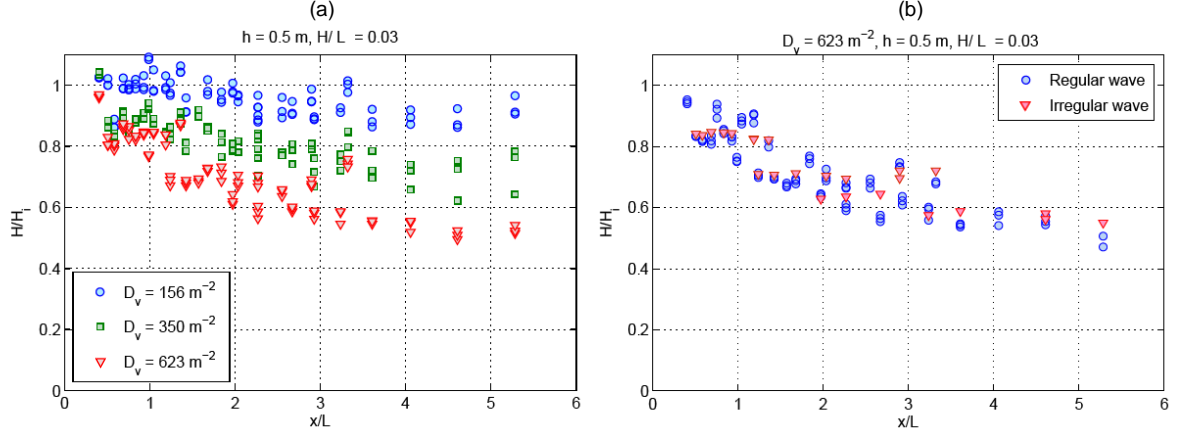


Figure 7. Wave heights within model vegetation for (a) regular and (b) irregular waves.

Figure 8 shows video analysis and wave gauge data for six different vegetation configurations. The solid lines in these plots are the smoothed time-averaged wave heights estimated from average frame analysis. It can be seen that the wave heights based on video analysis were similar to wave gauge data at fixed locations. The primary cause of uncertainty in the video data is due to the cross-tank variations in the water surface, mainly cross-tank seiche. The water surface considered in the video recordings was the interface visible to the camera along the side wall, while the wave gauges were mounted at the tank's centerline. The cross-tank resonant frequency was avoided in order to minimize this source of error. Other sources of uncertainty include camera alignment and distortion errors. However, the water surface displacement comparison given in Figure 4 shows that there was no phase shift between the two signals which indicates that uncertainty due camera distortion and alignment was minimized with the camera correction procedure.

Waves propagating through vegetation lose energy due to the work they do on the vegetation. Dalrymple et al. (1984) approximated the wave height evolution through a vegetation field based on conservation of energy for linear monochromatic waves. In a similar way, the wave height evolution here is expressed in terms of dimensionless values with the following model:

$$\frac{H}{H_i} = \frac{1}{1 - \alpha(x/L)} \quad (2)$$

where α is the damping factor. The model defined by Equation 2 is fitted to the experimental data in Figure 8.

Two important external effects had to be considered while evaluating the wave attenuation through the vegetation field inside the wave tank. One is the partial standing wave due to the reflected waves from the wave absorber at the end of the wave tank, and the other is wave attenuation due to the side walls, geometric imperfections, and nonlinearities. Even through the wave absorber was relatively short compared to the wave lengths used here; reflection was less than 10% for all of the runs. Yet, oscillations around the fitted curve indicate the existence of

reflected waves. It is not possible to estimate the wave reflection from the wave gauge data, but the video data clearly show the nodes and antinodes of the partially standing waves. This difference should be expected since wave height readings at a limited number of fixed points can lead to unrealistic results due to aliasing in the presence of standing waves. For example, Figure 8e shows that the second gauge reading coincided with an antinode and the third gauge with a node.

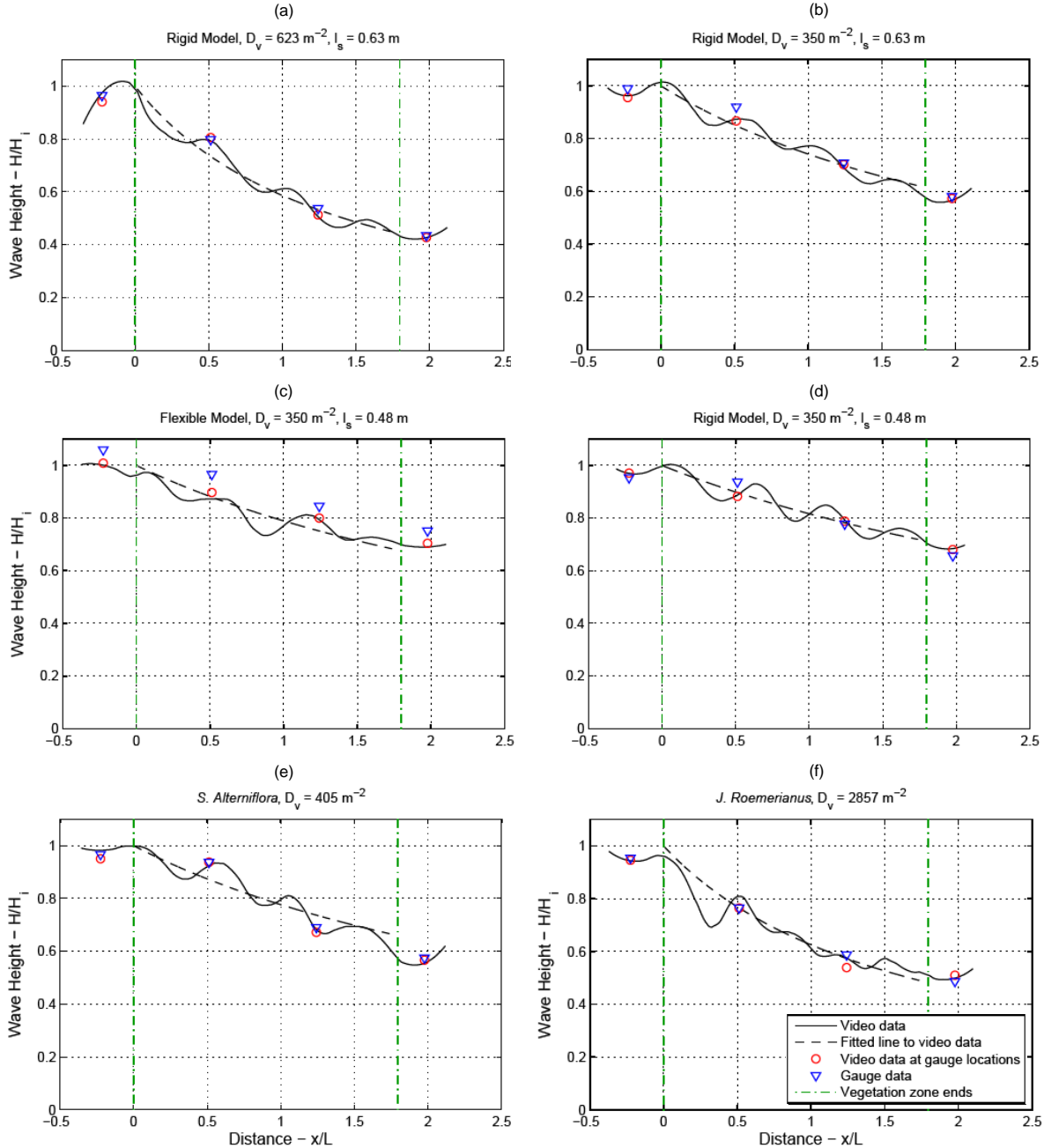


Figure 8. Wave height evolution along model and live vegetation configurations. ($T = 1.2 \text{ s}$, $H_i = 0.1 \text{ m}$, $h = 0.5 \text{ m}$.)

Wave setup is the water level rise due to the momentum transfer to the water column during wave-breaking process. The results of a typical experiment are shown in Figure 9. The estimated wave height transformation along the plane beach is compared with gauge data in Figure 9a. The solid line is the smoothed time-averaged wave height profile estimated from the transformed average frame (**J**) using the threshold defined by Equation 2. The mean and maximum differences between wave heights estimated through video data and wave gauge data were 4 mm and 5 mm which show a good agreement between the two measurement techniques. Figure 9b shows the mean water level and wave height envelope along the beach profile. The breaking point is assumed to be the station where the wave crest line in Figure 9b becomes maximum. The mean maximum differences between the wave gauge and video analysis results for mean water level was 1.2 mm and 3 mm.

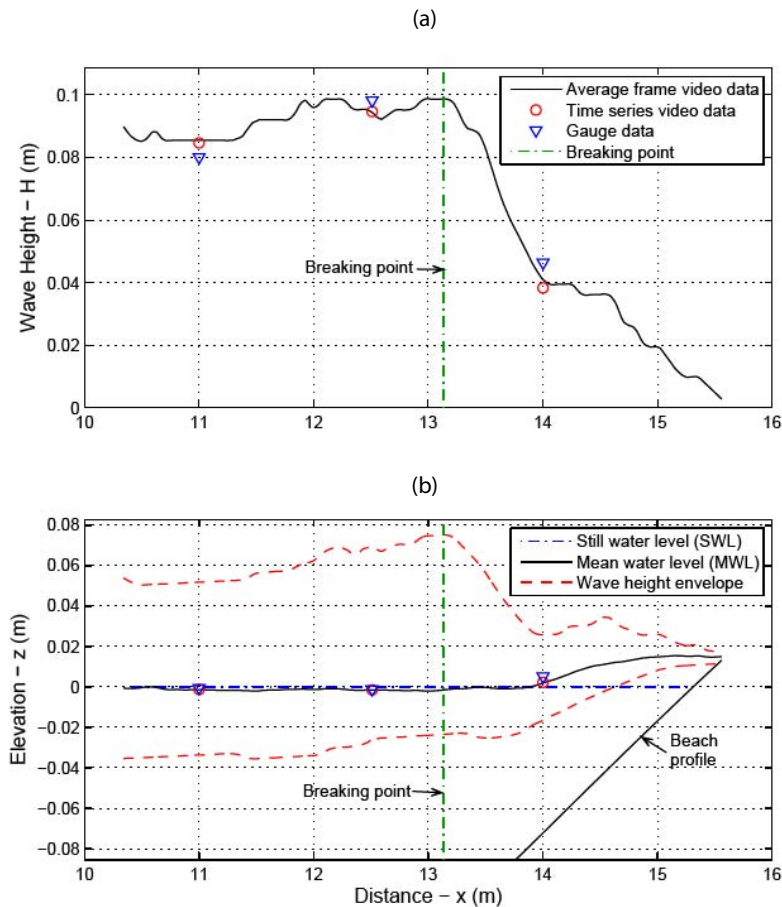


Figure 9. (a) Wave height transformation and (b) mean water level along the plane sloping beach ($T = 1.2$ s, $H_i = 0.09$ m, $h = 0.4$ m and slope = 1:20).

CONCLUSION

The attenuation of waves as a function of vegetation type, density, and height were analyzed in a laboratory wave tank. A video camera was used to record the water surface profile and a video analysis procedure was developed to estimate the evolution of wave height through model

and live vegetation. The video data analysis was validated by comparison with stationary wave gauge data for wave transformation through vegetation. The method was also used to estimate wave setup over a plane sloping beach. The water surface displacements estimated by the video analysis at gauge locations were in agreement with the gauge data. The video analysis method provided improved resolution for assessment of wave height evolution through different types of vegetation. The method will be used in a detailed study on the estimation of drag coefficient and to provide additional information on wave transformation through various types of vegetation.

ACKNOWLEDGMENTS

The authors would like to thank Jeffrey Diers and Glenn Gray for their assistance throughout the experiments. This research was funded by the Department of Homeland Security-sponsored Southeast Region Research Initiative (SERRI) at the Department of Energy's Oak Ridge National Laboratory

REFERENCES

- Asano, T., Tsutsui, S., and Sakai, T. (1988). "Wave damping characteristics due to seaweed" Proc., 25th Coastal Engineering Conf. in Japan, 138-142.
- Augustin, L.N., Irish, J. L. and Lynett, P. (2009) "Laboratory and Numerical Studies of Wave Damping by Emergent and Near-Emergent Wetland Vegetation" Coastal Engineering **56**, 332-340.
- Bonmarin, P., Rochefort, R. and Bourguel, M., (1989) "Surface Wave Profile Measurements by Image Analysis" Experiments in Fluids, **7**(1):17:24.
- Dalrymple, R. A., Kirby, J. T. and Hwang, P. A. (1984) "Wave Diffraction Due to Areas of Energy Dissipation" J. Waterway, Port, Coastal, and Ocean Eng. **110** (1): 67-79.
- Dean, R. G. and Bender, C. J. (2006). "Static Wave Setup with Emphasis on Damping Effects by Vegetation and Bottom Friction." Journal of Coastal Engineering. **53**:149-156.
- Erikson, L. H., and Hanson, H., (2005) "A Method for Extracting Wave Tank Data Using Video Imagery and its Comparison to Conventional Data Collection Techniques" Computers and Geosciences, 31(3): 371-384.
- Gambi, M. C., A. R. M. Nowell and P. A. Jumars (1990). "Flume observations on flow dynamics in *Zostera marina* (eelgrass) beds." Marine Ecology Progress Series, **6**:159-169
- Longuet-Higgins, M. S. (1952) On the Statistical Distribution of the Heights of Sea Waves, Journal of Marine Research, **11**(3): 245-266.
- Nepf, H. M. (1999) "Drag, Turbulence, and Diffusion in Flow Through Emergent Vegetation." Water Resources Research, **35**(2): 479-489.
- Wu, W. (2007). Computational River Dynamics, Taylor & Francis, p. 508.